

Inherent Reactivity of Praseodymium-Modified Ceria-Zirconia Catalysts for Oxidation of Soot

Cimi A. Daniel^{1*}, Reni George² and S.Sugunan³

¹Department of Chemistry, St. Thomas College, Kozhencherry, India

²Department of Chemistry, Mar Thoma College, Thiruvalla, India

^{1,3}Department of Applied Chemistry, Cochin University of Science and Technology
Cochin-682022, Kerala, India

Corresponding author (e-mail: danielcimi@gmail.com)

In this investigation, modified and pure ceria-zirconia catalysts were prepared by a surfactant-assisted hydrothermal method. Analytical techniques such as Powder X-ray diffraction (XRD), BET-BJH-surface area, Thermogravimetry/differential thermogravimetry (TG/DTG), Raman spectroscopy (RS), X-ray photoelectron spectroscopy (XPS), transmission electron microscopy (TEM) and Temperature Programmed Reduction (TPR) were utilized to characterize the structures of the prepared catalysts. The formation of a cubic fluorite structure of ceria-zirconia was inferred from XRD analysis. The oxidation states of the metals present were studied using XPS. The objective of this work was to investigate the effect of cerium content and the influence of praseodymium in promoting the soot combustion activity of ceria-based catalysts. Our study showed that the order of activity depends on the amount of the cerium and modified metal. Modification of the ceria-zirconia catalysts with praseodymium enhanced the catalytic activity to a great extent. Notably, the reactivity of the soot combustion reaction was found to correlate with the improved redox properties and the synergistic effect of praseodymium and the ceria component.

Key words: Soot oxidation; ceria-zirconia; praseodymia modified ceria-zirconia; tight contact

Received: November 2020; Accepted: February 2021

Diesel particulate matter (or soot) emitted from diesel engines poses a serious problem to human health and the environment. The usual method of removing diesel particulate matter is to trap the DPM using a diesel particle filter (DPF) in the exhaust. DPFs can reduce 70 to 95 wt % of the particulate matter mass. As the filter collects DPM, it builds up backpressure resulting in decreased fuel economy and possible engine and filter failure. As a result, the trapped DPM needs to be converted by gasification/oxidation to carbon monoxide (CO) and carbon dioxide (CO₂). The major problem associated with this is the difficulty in obtaining spontaneous and self-propagating regeneration of particulate filters during soot combustion. The chemical process for regeneration of these filtration systems is the oxidation kinetics of the carbon. Soot can be oxidized only at temperatures higher than 550°C or 600°C with the oxygen contained in the exhaust gas. Generally, the exhaust gas temperature does not exceed 400°C during normal driving conditions [1]. A workable solution is to increase the exhaust gas temperature, which can be done using another energy source that bears additional costs. Furthermore, high regeneration temperatures could easily damage the filter. Therefore, the preferred way for regeneration is to develop efficient and thermally-stable catalysts.

Platinum group metal (PGM) catalysts are very active in the soot oxidation reaction [2]. The disadvantages of Pt are its high cost, scarcity and production of sulfate particulates. These problems inspired researchers to develop different non-noble metal catalysts such as single and mixed metal oxides, perovskite as well as spinel-type oxides for diesel exhaust treatment [3]. Atribak et al. found that CeO₂ was more active than ZrO₂ for soot oxidation experiments carried out under tight contact between the soot and the catalyst. This was ascribed to the generation of highly-active oxygen in the lattice due to the oxygen exchange between gas-phase O₂ and oxygen in the oxide framework [4]. Bueno et al. used an advanced TAP reactor for the first time to study CeO₂-catalyzed soot oxidation using labelled oxygen [5]. In the presence of the catalyst, it was shown that the gas-phase labelled oxygen replaces the non-labelled lattice oxygen of CeO₂ creating highly active oxygen which upon reacting with soot gives CO and CO₂. The creation of such active oxygen species started at 400°C, resulting in a decreased soot oxidation temperature, whereas oxidation generally takes place above 500°C in a non-catalyzed reaction. Nevertheless, pure ceria is susceptible to sintering thereby deactivating the catalyst at high temperatures. Therefore, the thermal

stability of ceria is a prerequisite before it can be used for catalytic applications. By maintaining the fluorite structure of ceria with thermal stability, the electronic and catalytic properties can be enhanced. This can be achieved by modifying ceria with rare earth elements or transition metals.

The catalytic efficiencies of ceria-zirconia and ceria-hafnia nanocomposite oxides for soot oxidation have been compared and it was found that the $T_{1/2}$ temperatures for CZ and CH soot mixtures are 514 °C and 409 °C, respectively [6]. Neelapala et al. [7] reported that Cr-doped ceria catalysts prepared by sol-gel synthesis could reduce the soot oxidation temperature (T_{50}) to 450 °C when compared to uncatalyzed soot (600 °C) whereas pure ceria exhibited a T_{50} of 405 °C. The ceria-zirconia sample was prepared by the co-precipitation method and tested in the oxidation of carbon soot at different oxygen partial pressures. T_{50} as a function of the reaction atmosphere was studied for all the investigated catalysts and was found to be around 550, 400 and 370 °C under an inert, 1% O_2/N_2 and air atmosphere respectively [8]. A set of ceria, ceria-zirconia and ceria-zirconia-praseodymia catalysts, prepared by solution combustion synthesis has been studied in soot oxidation reactions and T_{50} , the temperature at which 50% conversion of soot takes place, was found to be 451, 469 and 444 °C, respectively [9]. They reported that praseodymium-doped ceria exhibited enhanced oxygen vacancies by increasing cerium redox sites which in turn affects the catalytic activity, but the sizes of crystallites synthesized were in the range 13–23 nm with surface areas less than 40 m²g⁻¹. Jen et al. [10] found that the insertion of 5 wt.% praseodymium increased the thermal stability of $Ce_{0.7}Zr_{0.3}O_2$.

Only a few studies involving praseodymium-modified ceria-zirconia prepared by a hydrothermal method and modified by a wet impregnation method were screened for the soot oxidation reaction. Our strategy was to prepare ceria-zirconia by a hydrothermal templated method and praseodymium-modified ceria-zirconia was achieved by a wet impregnation method. By this method, preparation of a layer of active matter on the catalyst's surface was easy, inexpensive and the final property of the catalyst could be controlled. Various reaction parameters were studied and reaction conditions were optimized.

EXPERIMENTAL PROCEDURE

1. Catalyst Preparation and Characterization

Ceria-zirconia mixed oxide was prepared by adopting a surfactant-assisted method using cerium nitrate, $Ce(NO_3)_3 \cdot 6H_2O$ and zirconium oxychloride, $ZrOCl_2 \cdot 8H_2O$ as precursors. Each precursor, in the required quantity,

was separately dissolved in deionized water and then blended together. This mixture was added slowly to cetyl trimethyl ammonium bromide solution (surfactant/cerium nitrate=3.5 molar ratio) with stirring. Ammonium hydroxide (28wt%) was then added dropwise into the mixture until precipitation was complete (pH = ~11). The precipitate obtained was loaded into a stoppered Teflon bottle and heated hydrothermally at 100 °C for 48 hours. The resulting slurry was filtered and washed with distilled water. The mixed hydroxide paste was allowed to dry at 80 °C for 12 hours, and then calcined at 500 °C for 4 hours. For comparison purposes, CeO_2 - ZrO_2 mixed oxides with different mole ratios, ceria: zirconia 2:1, 1:1, 1:2 (mole ratio based on metal salt) were prepared. The modification with the transition metal is done with a CZ ratio of 1:1. The praseodymium-modified ceria-zirconia catalyst was prepared by wet-impregnation of the ceria-zirconia support with the required amount of aqueous solution of praseodymium (III) nitrate hexahydrate. This mixture was stirred for 6 hours and then dried at 110 °C for 4 hours. It was then powdered and calcined at 400 °C to obtain praseodymium-modified ceria-zirconia oxide. The support catalysts prepared for the present work are labelled C2Z1, CZ and C1Z2. Praseodymium modified ceria-zirconia (with 4, 8 and 12 weight% of praseodymium) are 4PrCZ, 8PrCZ and 12PrCZ.

ICP-AES analysis was done on a Thermo electron IRIS INTERPID II XSP DUO model. Powder XRD of the prepared samples was done on a Bruker AXS D8 Advance model with Ni filtered Cu $K\alpha$ radiation (λ -1.5406 Å) within the 2θ range 5-80° at a speed of 2°/min. Determination of surface area and pore size distribution of the samples was done with a Micromeritics Tristar 3000 surface area and porosity analyzer. Prior to analysis, the samples were degassed at 90 °C for half an hour and 300 °C for three hours. Thermal analyses of the synthesized samples were carried out on a Perkin Elmer TGA (Delta series TGA 7) with a steady heating rate of 20 °C/min. Raman spectra were recorded on a Horiba Jobin Ivan Lab Ram HR system at a spatial resolution of 2 mm in a backscattering configuration. The 514.5 nm line of an Argon ion laser was used for excitation. XPS spectra were recorded on an electron spectrometer equipped with Thermo VG Clamp -2 Analyzer and a Mg $K\alpha$ X-ray source (1253.6 eV, 30 mA x 8 kV). A thin sample wafer of 12 mm diameter was used for measurements. TEM analyses were performed on a CM200 (Philips) with an operating voltage 20-200kV providing a resolution of 2.4 Å. TPR profiles of the calcined samples were obtained on a Micromeritics TPR apparatus which was interfaced with a computer. The sample, placed in a U-shaped quartz tube, was first purged in a He flow for 1h and then cooled to ambient temperature. TPR profiles were taken of the degassed sample by passing it through a 10% H_2/Ar gas mixture in which the sample was heated at a constant rate of 10 °C/min from room temperature to 800 °C.

Table 1. Elemental composition of prepared catalysts

Catalysts	Composition (atom %)					
	Theoretical			Experimental		
	Ce	Zr	Metal	Ce	Zr	Pr
C2Z1	56.6	43.4	--	64.1	35.9	--
CZ	39.5	60.5	--	43.4	56.6	--
C1Z2	24.6	75.4	--	34.7	65.3	--
4PrCZ	38.1	58.7	3.2	36.3	59.5	4.2
8PrCZ	36.9	56.8	6.3	33.2	59.4	7.4
12PrCZ	35.7	54.7	9.6	30.5	60.0	9.5

2. Catalytic Activity Measurement

Soot oxidation tests were performed with a Thermogravimetric analyzer (TGA7 Perkin Elmer). Carbon black (ISAF grade) was used as model soot. The activity studies were performed by using air as the source of oxygen. For tight contact experiments, each catalyst was accurately mixed with soot in an agate mortar to achieve a tight contact. For loose contact experiments, soot and the catalyst were mixed with a spatula. For the TG measurements, around 7 mg of the mixture was heated at a constant rate (20°C/min) from room temperature to 850°C, while the gas flow was kept fixed at 400 ml/min. For evaluating activity, we used the light-off temperature, T_{50} .

RESULTS AND DISCUSSION

1. Textural and Structural Characterization

Table 1 gives the amounts of Ce, Zr and praseodymium present in each sample. From this, it is clear that experimental atom % values are in agreement with theoretical values.

The prepared materials show XRD patterns (Fig.1) corresponding to the cubic fluorite structure [11]. No XRD patterns pertaining to ZrO_2 is observed. This indicates that cerium and zirconium ions are uniformly distributed in the structure to form a homogeneous solid solution thereby stabilizing the fluorite structure by zirconia substitution [12]. The characteristic peaks of pure ceria are seen at 2θ values of 28.5°, 33.0°, 47.5°, 56.5° corresponding to the planes (111), (200), (220) and (311) respectively with space group Fm3m (JCPDS database (75-0162)). These peaks shifted to higher values as the Zr content increased, which is in agreement with the literature [12]. The shift of peaks towards higher 2θ values is due to the smaller ionic radius of Zr^{4+} (0.84 Å) in comparison with that of Ce^{4+} (0.97 Å).

The XRD patterns of Pr-modified catalysts are presented in Fig.1 (b). These XRD patterns can be indexed to the fluorite structure with a space group Fm3m. Interestingly, the XRD pattern due to crystalline praseodymia is not noted. The fact that we could not trace any crystalline phase of praseodymia even on increasing the Pr content to 12 wt % indicates that amorphous microcrystals of praseodymia phase are well-dispersed on the given support. The existence of highly-dispersed praseodymia on the ceria-zirconia surface is indicated by the fact that there is not much change in the lattice parameter.

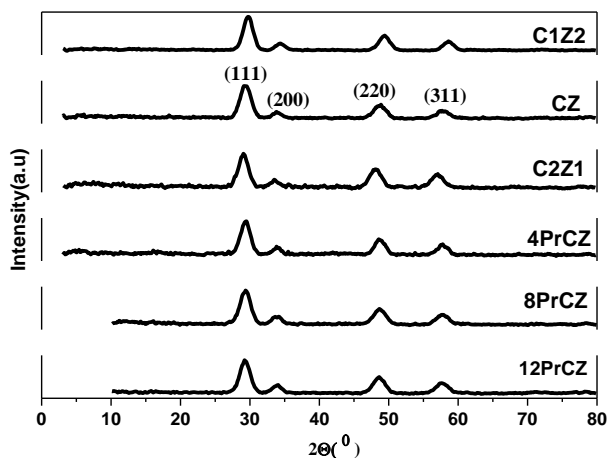


Figure 1. XRD diffraction patterns of ceria-zirconia and praseodymium-modified ceria-zirconia catalysts

Crystallite size measurements were also carried out using the Scherrer equation. It was found that the crystallite size of the pure CZ catalyst was 4.35 nm. Upon modification, it became 4.94, 4.95 and 4.86 nm for 4PrCZ, 8PrCZ and 12PrCZ respectively.

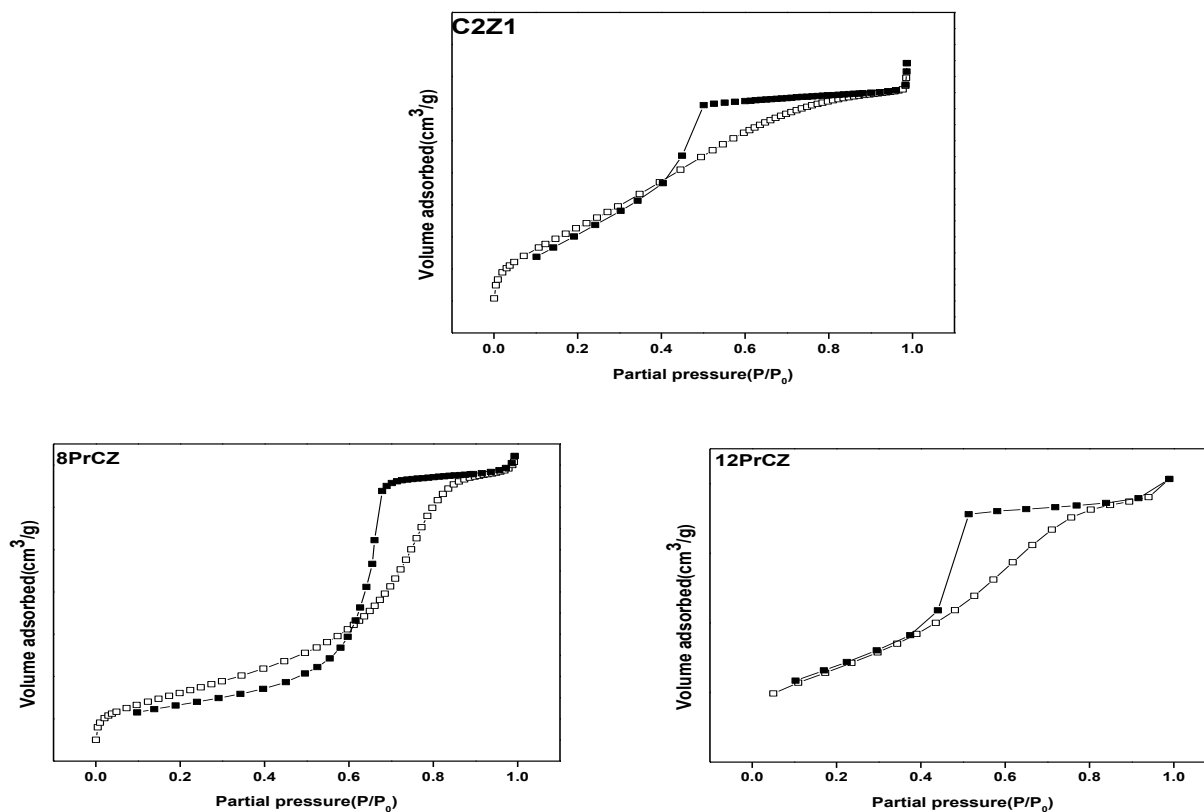


Figure 2. N₂ adsorption/desorption isotherms of ceria-zirconia and praseodymium-modified ceria-zirconia catalysts

Pure ceria-zirconia, CZ, possesses a high surface area of 132 m²/g. Increasing ceria or zirconia content decreases the surface area. For C2Z1, it is 125 m²/g, whereas for C1Z2, it becomes 76 m²/g. Surface area decreases upon modification of the ceria-zirconia support with praseodymium. This may be due to the blocking of the pores. The surface area becomes 91, 59 and 49 m²/g for 4PrCZ, 8PrCZ and 12PrCZ respectively. As the amount of Pr increases, more pore-plugging takes place which in turn reduces the surface area of the modified catalysts. As can be noted from Fig.2, all the adsorption-desorption isotherms can be classified as type IV, typical of mesoporous material. The shape of the curve indicates the absence of a narrow pore size distribution. According to IUPAC classification, the hysteresis loop is of type H2 with a relatively steep desorption branch in the range of relative pressure $P/P_0 = 0.4-0.5$. This hysteresis loop is typical for a wormhole-like structure [13] indicating a complex mesoporous structure.

The TG and DTG curves obtained for the CZ sample are shown in Fig.3. Two weight loss events are observed in the thermogram. The first loss occurs at around 170°C which may correspond to the dehydration of physically adsorbed water and loss of water held on the surface by hydrogen bonding. The second weight

loss at around 250°C is due to the decomposition of cetyl trimethyl ammonium bromide surfactant. As seen in the figure, the offset temperature of surfactant removal is around 370°C. It has been reported that thermal degradation of pure CTAB showed a weight loss between 180–340°C [14]. No further weight loss was observed, confirming the structural stability of the prepared catalyst.

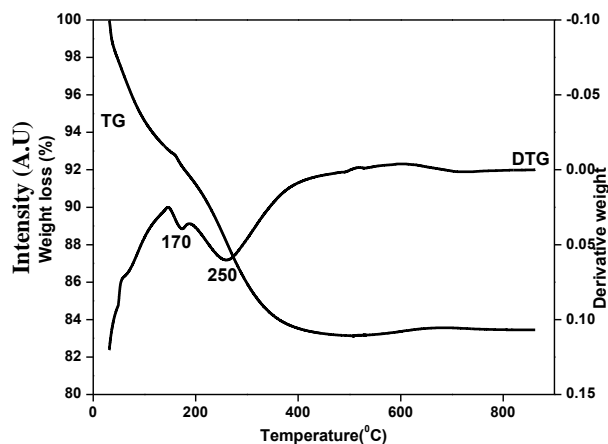


Figure 3. TG/DTG curve of ceria-zirconia catalysts

Raman bands reflect both surface and bulk information due to the weak absorption of samples in the visible range. Fig.4 shows the Raman spectra of mixed ceria-zirconia oxides. It has been reported that the Raman spectrum of bare CeO_2 has a single band centered at around 465 cm^{-1} that corresponds to the single allowed Raman mode (F_{2g}) of fluorite-type structures [15, 6]. In line with reported studies, the spectrum pertaining to C2Z1 shows a profile similar to that observed for pure ceria with a single predominant band at 465 cm^{-1} . This band corresponds to the triply degenerate F_{2g} mode and can be viewed as a symmetric breathing mode of oxygen atoms around cerium ions [16]. These vibrational modes occur with three equivalent motions of oxygen atoms on the three axes. F_2 mode splits into one symmetric component F_{2g} , which only involves movements of the oxygen atoms (Raman active), and another asymmetric F_{1u} which involves movements of both the oxygen and cerium atoms (IR-active) [17].

It is clear from Fig. 4(a) that the intensity of the strong band at $\sim 465 \text{ cm}^{-1}$ decreased considerably for CZ compared to C2Z1. Moreover, when the Zr content increased further in C1Z2, the main peak in the Raman spectra broadened considerably whereas the six broad bands characteristic of the tetragonal symmetry occurred at about 125, 206, 310, 465, 590 and 640 cm^{-1} . Escribano et al. suggested that this may be due to the presence of tetragonal and cubic solid solution phases though the cubic phase is still largely predominant [17]. However, it is difficult to predict the co-existence of both phases due to the broadness and overlapping of ZrO_2 and CeO_2 bands [12]. It is also supposed that the reduced intensity of the predominant Raman peak may be due to the strong interaction between zirconium and cerium oxide species occurring during the high-temperature calcination process which resulted in the formation of oxygen vacancies by the reduction of cerium [18].

A small shoulder peak at approximately 600 cm^{-1} is attributed to oxygen vacancies in the ceria lattice [6, 19]. This peak can be assigned as the non-degenerate Longitudinal Optical (LO) mode of ceria arising due to the relaxation of symmetry rules. The presence of oxygen vacancies is likely to enhance the catalytic performance of these systems. The weak band observed at around 300 cm^{-1} for C1Z2 can be ascribed to the displacement of oxygen atoms from their ideal fluorite lattice positions [17]. The Raman spectra for 8PrCZ (Fig.4(b)) revealed one main peak centred at about 468 cm^{-1} which is typical of the F_{2g} Raman active mode of the fluorite-structured materials. For Pr-modified catalysts, no characteristic peaks are found due to Pr oxides, indicating that Pr is well dispersed in the support.

The prepared catalysts were analysed by XPS to investigate the oxidation state of the elements. The photoelectron peaks of Ce 3d, Zr 3d and O 1s of C1Z2 are depicted in Fig.5[(a), (b), (c)] respectively. The Ce 3d core-level spectra of ceria is complicated, not only because of multiple oxidation states but also because of the mixing of Ce 4f levels and O 2p states during the primary photoemission process [20]. Peaks labeled as 'v' correspond to Ce $3d_{5/2}$ contributions and those denoted as 'u' represent the Ce $3d_{3/2}$ contributions which are reported elsewhere [12]. The peaks observed in the XPS spectrum are in agreement with the literature [21, 22]. The four main $3d_{5/2}$ features at 880.6, 884.9, 891.0, and 898.6 eV correspond to V, V', V'' and V''' components, respectively. The main $3d_{3/2}$ features about 900.6, 903.1, 909.8, and 914.5 eV correspond to U, U', U'' and U''' components, respectively. The peaks of V' and U' represent the $3d^{10}4f^1$ initial electronic state belonging to the unique photoelectron features of the Ce^{3+} state. The others are satellite peaks. The main peaks of V''' and U''' represent the $3d^{10}4f^0$ initial electronic state corresponding to the Ce^{4+} ion.

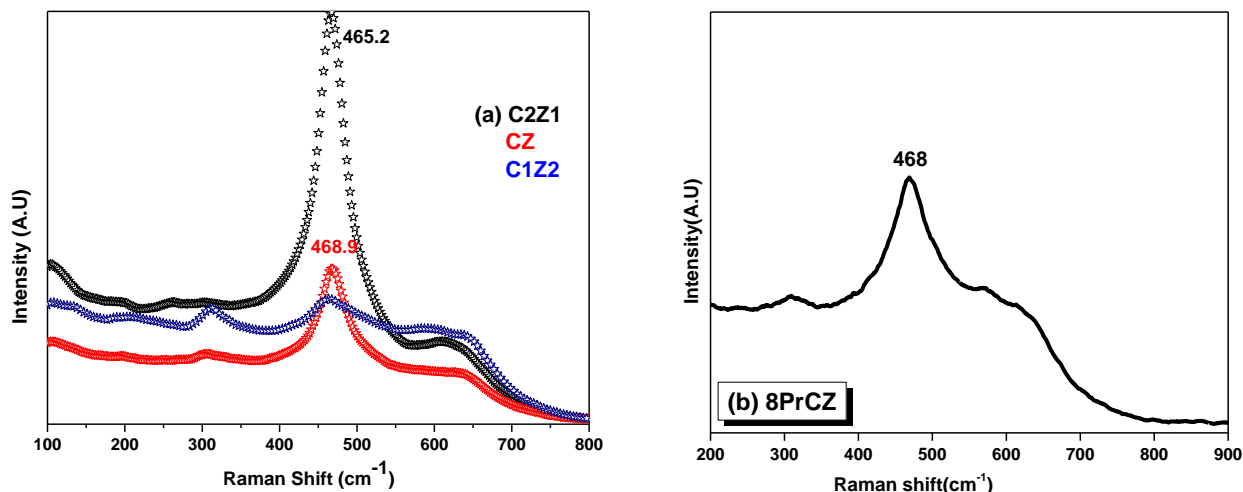


Figure 4. Raman spectra of ceria-zirconia and praseodymium modified ceria-zirconia catalysts

Thus C1Z2 exhibited peaks that are due to the presence of both Ce^{4+} and Ce^{3+} ions, implying that cerium is present at the surface in both +4 and +3 oxidation states [18]. It is observed from the core level XP spectra of Zr 3d that the peaks at 182.6 and 184.9 eV correspond to Zr $3d_{5/2}$ and Zr $3d_{3/2}$, respectively (Zr^{4+}). The difference in the binding energies (BE) between the Zr $3d_{5/2}$ and Zr $3d_{3/2}$ photoemission feature is 2.3 eV, which is in agreement with the literature [23]. The position of the primary O 1s feature found at 530.1 eV is attributed to the lattice oxygen associated with the C1Z2 metal oxides.

The spectrum for the Pr modified catalyst is rather broad. Deconvolution of the peaks allows

unambiguous identification of the oxidation states of the metals. According to the literature, in the spectrum of Pr two sets of 3d spin-orbit multiples are observed at binding energies of ~ 933 and ~ 953 eV corresponding to the $3d_{5/2}$ and $3d_{3/2}$ electrons of Pr [22, 24]. Because of the high redox property of PrO_2 , there is a possibility of the coexistence of mixed-valence +3 and +4 cations ($\text{Pr}^{4+}/\text{Pr}^{3+}$) at equilibrium for the stable Pr_6O_{11} ($4\text{PrO}_2 \cdot \text{Pr}_2\text{O}_3$). As expected, the $3d_{5/2}$ sublevel consists of two peaks at 933.4 and 929.2 eV which can be assigned to Pr^{4+} and Pr^{3+} respectively. Two features of $3d_{3/2}$ observed at 953.6 and 950.1 eV correspond to Pr^{4+} and Pr^{3+} respectively. This indicates that the prepared sample contains both +3 and +4 oxidation states of praseodymium at the surface region.

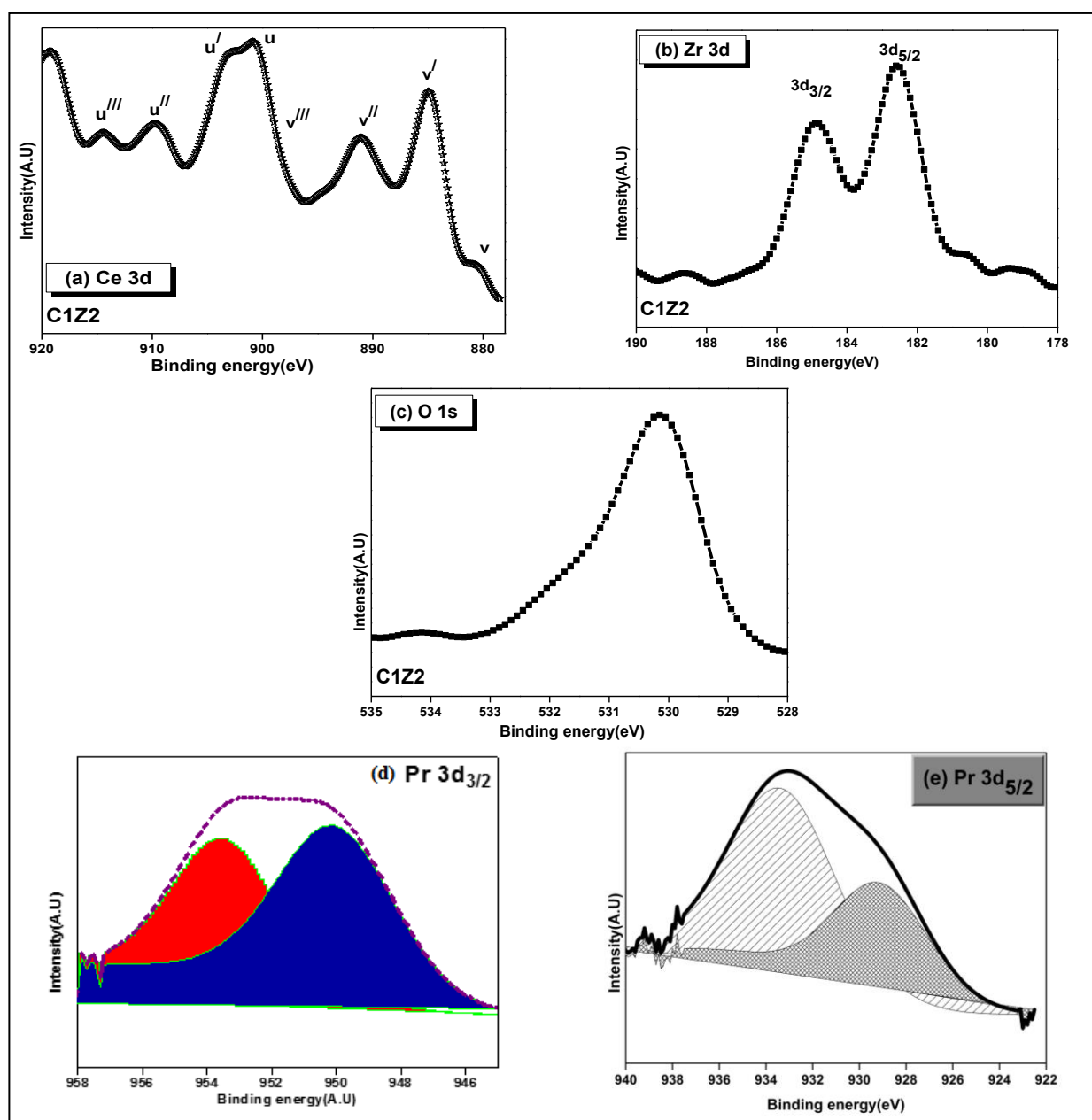


Figure 5. XPS spectra of ceria-zirconia and praseodymium modified ceria-zirconia catalysts

Micrographs showed that the sample was in polycrystalline form and consisted of small crystallites. The lattice fringes of nanocrystalline material was clearly detected by the high-resolution TEM image (Fig.6). The HRTEM image of the CZ sample

indicated that the particles crystallized as a cubic fluorite-type structure of ceria, exposing preferentially the crystal plane (111) with a d spacing of 3.1 Å, in addition to the (200) plane with 2.7 Å nm interplanar spacings [13].

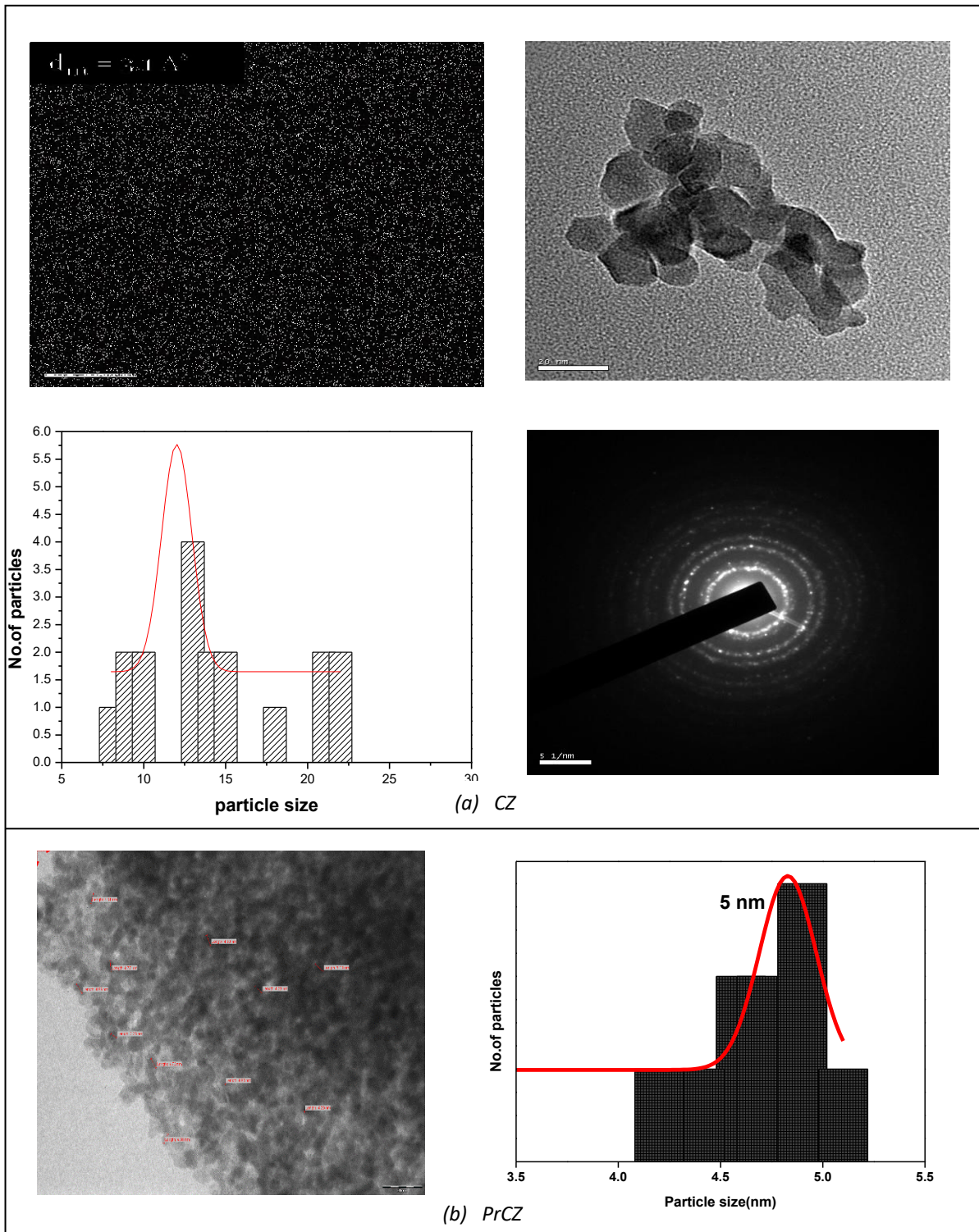


Figure 6. TEM images and particle size histograms of (a)ceria-zirconia and (b) PrCZ

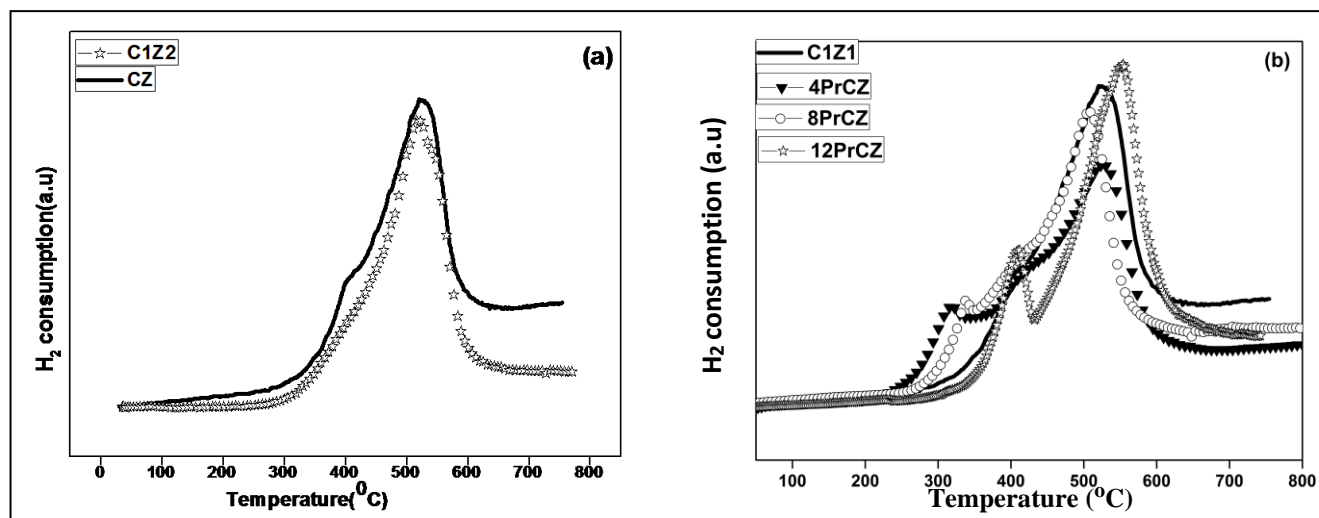


Figure 7. TPR profile of ceria-zirconia and praseodymium modified ceria-zirconia catalysts

The images revealed a porous structure of the oxide. As observed from these figures, an agglomeration of dense nanoparticles has taken place. Statistical analysis of these micrographs was carried out. Particle size histograms can be plotted from TEM images and these reveal that the average particle size is 12 nm for CZ and 5 nm for PrCZ, as shown in Fig.6. These results are in good agreement with those obtained from XRD peak broadening measurements.

The selected area electron diffraction (SAED) pattern of the CZ sample exhibited concentric rings that are essentially continuous, implying that the sample consisted of many very small crystallites (Fig.6(a)). Inter-planar spacings were calculated from the pattern and can be indexed to a cubic fluorite phase. The SAED pattern also confirms the formation of the thermodynamically most stable (111) surface plane. The shapes of the particles observed from TEM images are almost similar to those usually seen in previous work on ceria-zirconia specimens [25, 6]. Transmission images confirm that the adopted preparation method is favorable for maintaining the highly-ordered structure.

H₂-TPR experiments were performed to analyze the reducibility of the catalysts. TPR profiles are plotted in Fig.7. TPR patterns of the ceria-zirconia support are given in Fig.7 (a). It is reported in the literature that two peaks were observed in the TPR patterns of some ceria-based catalysts which were assigned as (i) the reduction of the most easily reducible surface oxygen of ceria species and (ii) the removal of oxygen from bulk ceria [12]. In the case of ceria-zirconia mixed oxides, researchers suggest that it is difficult to differentiate between surface and bulk reduction as both reduction peaks appear together i.e.,

both reductions occur concurrently [20]. For the CZ sample, the temperature maxima for the reduction was around 521°C. In addition to this, there was a small hump observed at a lower temperature region around 405°C. This can be attributed to the reduction of surface Ce⁴⁺ to Ce³⁺ [22]. In line with earlier findings, as the Zr content increases (for C1Z2), one TPR peak at 516°C was observed. The TPR profiles of 4, 8 and 12 wt % Pr modified catalysts are shown in Fig.7 (b). For each sample, there were two reduction peaks. In praseodymia-modified ceria-zirconia catalysts, there was a well-defined peak at lower temperatures whereas only a hump was observed for ceria-zirconia catalysts. This refers to the reduction of surface oxygen and it has been reported that doping with praseodymium favors the weakening of Ce–O bonds [9]. Pr-modified CZ was the better reducible catalyst compared to the pure ceria-zirconia, based on the two reduction peaks. It was also reported that as T_{max} increases, dispersion of the metal decreases. The crystallites formed may not have a strong interaction with the support oxide.

2. Catalytic Activity of Ceria-zirconia-based Materials

2.1. Effect of Catalyst

In order to study the effect of the catalyst, the combustion of carbon was performed without a catalyst. Fig.8 shows the soot conversion graph which is calculated from TG experiments. There is a significant difference observed between the non-catalyzed reaction of carbon and oxygen as compared to the catalyzed reaction. Noncatalytic combustion of carbon took place at about 570–670°C with T₅₀ at 634°C. The T₅₀ value for the reaction with the CZ catalyst was 496°C, which showed the efficiency of the

catalyst. The high catalytic activity of ceria-zirconia for soot oxidation was attributed to the presence of surface/bulk oxygen to oxidize soot, and the oxidation of carbon occurs at the carbon/CZ interface with the formation of an oxygen vacancy, as mentioned in previous reports [26,8].

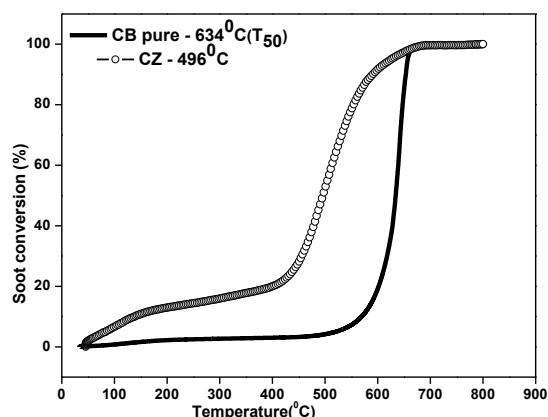


Figure 8. Effect of ceria-zirconia catalyst on soot oxidation.

2.2. Effect of Contact between Catalyst and Soot

The contact between soot and catalyst is a key factor in the process of catalyzed soot oxidation [27]. Van Setten et al. have described two modes of soot catalyst contact, loose (LC) and tight (TC) contact [28]. For this experiment the soot-catalyst mixture, in an appropriate ratio, was milled in an agate mortar for tight contact or mixed carefully with a spatula for loose contact. Loose contact mode can mimic a realistic contact between the soot and the catalyst in a DPF filter. This is for very simple practical use and relevant for kinetic laboratory studies. Even though tight contact conditions are a poor representation of real working conditions experienced by the catalyst deposited in a catalytic trap, tight contact conditions have the following features: (1) reflect the intrinsic characteristics of the catalysts (2) allow a rapid screen of catalysts in reproducible experimental conditions (3) provide higher reaction rates (4) help to obtain wider differences among catalyst activity, and so is useful for basic research [17]. Both contact conditions were tested for the present study.

To study the effect of contact, TG experiments were carried out with the 12PrCZ catalyst. (Fig.9). For tight contact experiments, the catalyst was accurately mixed with soot in a mortar in a 1:6 wt ratio. Catalyst and soot were mixed with a spatula in the same ratio for loose contact conditions. Samples prepared with tight contact showed soot oxidation at much lower temperatures than samples prepared with loose contact. This may be

ascribed to the increase of more available active oxygen in the reaction [29]. Loose contact did not cause a significant decrease in the soot oxidation temperature, consistent with reported literature [4]. The decrease of activity under loose contact conditions is due to the decrease of soot-catalyst contact. These studies support the fact that catalysts require physical contact to be active. Thus we have selected tight contact conditions for further optimization studies.

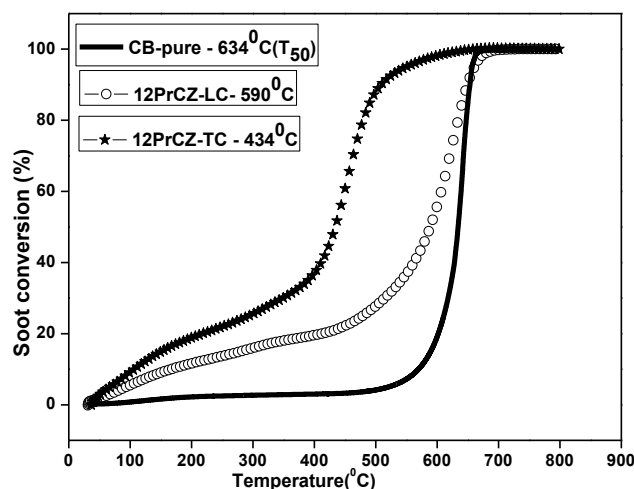


Figure 9. Effect of contact type on soot oxidation.

2.3. Effect of Catalyst Amount

Catalytic activity was compared for the soot:catalyst weight ratios of 1:2, 1:4, 1:6 and 1:8 under the same experimental conditions. 8PrCZ was studied for this purpose. Oxidation evaluation results are given in Fig.10. The results clearly demonstrate the activity of the catalyst as the soot oxidation is observed at a much lower temperature. In the presence of a catalyst, irrespective of the ratio, a decreased soot oxidation temperature is observed. The T_{50} value for non-catalyzed soot oxidation was 634°C. At a soot:catalyst ratio of 1:2, the T_{50} value was 506°C. There is not much reduction of oxidation temperature with a 1:4 ratio [18]. A reduction of around 40°C was achieved with a soot: catalyst ratio of 1:6. As the ratio increased further, no significant effect was observed. Therefore, a soot catalyst ratio of 1:6 was chosen for screening studies.

2.4. Effect of Ce: Zr Ratio

From Fig.11(a), it is deduced that the catalytic activity of the Ce:Zr catalysts with different Zr content follows the order: C2Z1 > CZ > C1Z2. It was reported that catalysts with a higher amount of cerium showed higher

activity than those with a lower amount [27]. CeO_2 has been suggested as a favorable soot oxidation catalyst as it accelerates the soot- O_2 reaction. Highly-labile surface oxygen is formed first by replacing CeO_2 lattice oxygen with gas-phase O_2 , which in turn reacts with soot [30]. This may be a reason for the higher activity of C2Z1. The low activity of C1Z2 is due to the lesser Ce amount and also a low BET surface area. However, activity does not show a positive trend with surface area. For instance, C2Z1 bearing a surface area of $125 \text{ m}^2/\text{g}$ exhibited better activity than CZ (which has a surface area of $132 \text{ m}^2/\text{g}$). It is worth noting that a linear relationship was observed between catalytic activity and Ce content. It may be concluded that the trend in activity is due to the mobility of lattice oxygen and also better exchange with gas-phase oxygen [31].

2.5. Effect of Impregnated Metal

Catalytic activity for soot oxidation was performed over Praseodymium-modified ceria-zirconia catalysts. Results are given in Fig.11(b). Almost all the catalysts show a decreased trend of soot oxidation temperature compared to the bare ceria-zirconia support. The best formulation for the reaction is 12PrCZ with a T_{50} value of 434°C . The presence of praseodymium has been shown to present considerable benefit to several catalyst formulations for soot oxidation. It is suggested to shift its oxidation state from $4+$ to $3+$, thereby exhibiting its promotional effect in the ceria-zirconia catalyst. The higher activity of Pr-modified catalysts can be correlated to the presence of both $\text{Ce}^{4+/3+}$ and $\text{Pr}^{4+/3+}$ ions which in turn make it a good catalyst for the soot oxidation reaction [30].

In diesel soot oxidation, the catalyst plays a significant role. The reaction, being exothermic in nature, generates heat that assists the catalytic oxidation of soot [32].

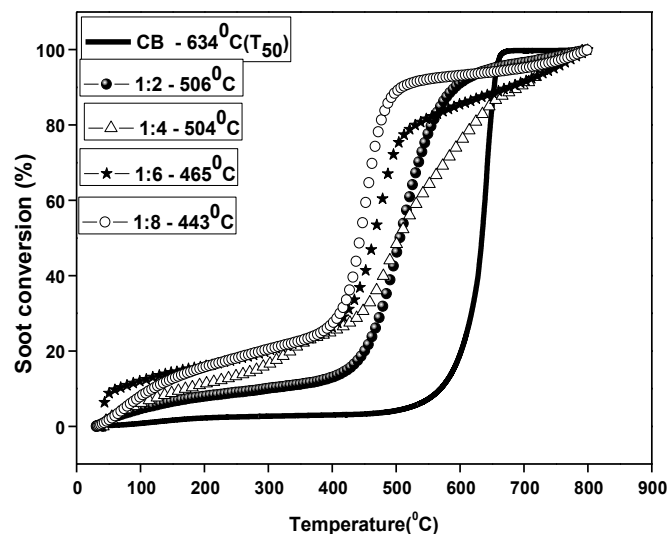


Figure 10. Effect of catalyst amount on soot oxidation.

The active oxygen transfer across the soot surface is suggested as a key issue for soot oxidation activity [33]. The catalyst containing an impregnated metal shows a significant lowering of carbon oxidation as compared to the bare support-catalyzed reaction. This suggests that the catalytic activity is also a feature of the modified metal component. Better activity is due to the synergistic effect of mixed oxide and metal nanoparticles. The existence of small metal oxide particles on the catalyst surface increases the number of contact points between the soot and the catalyst. Praseodymium-doped samples exhibited a lower $T_{1/2}$ of around 434°C . High praseodymium loading (12%) was more effective than low dosages. Within the series, the activity first decreased and then increased. This may be ascribed due to H_2 consumption [18].

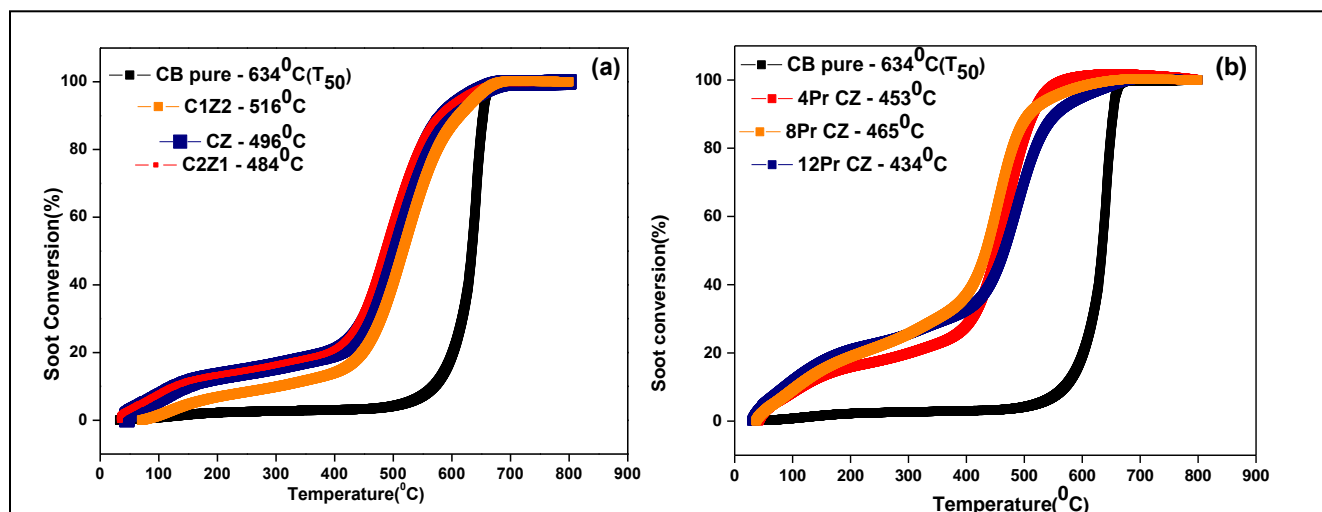


Figure 11. Comparison of catalysts for soot oxidation

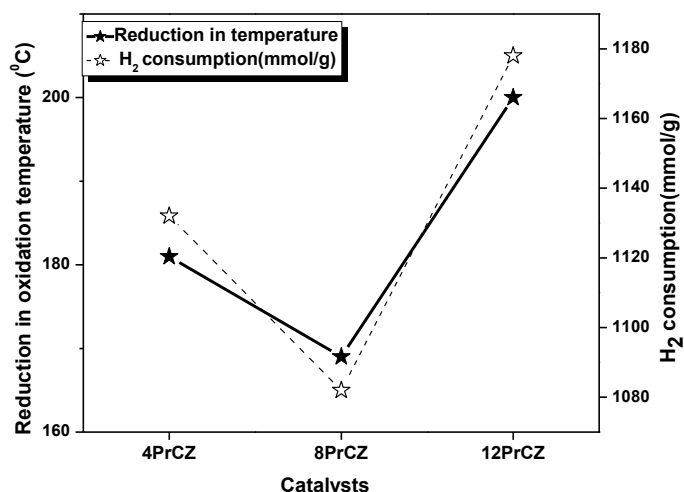


Figure 12. Relation between reduction in soot oxidation temperature and H₂ consumption

The reduction in soot oxidation temperature for PrCZs can be correlated with H₂ consumption as measured by the temperature-programmed reduction of H₂ (Fig.12). A drastic decrease in soot combustion temperature observed for 12PrCZ is due to the improved redox properties of the material. However, a detailed study of the mechanism of soot oxidation remains unexplored for modified ceria-zirconia catalysts.

CONCLUSION

Cerium-zirconium mixed oxides with good surface area were synthesized by the hydrothermal method using CTAB as a template. These mixed oxides calcined at 500 °C maintained a cubic phase of fluorite structure as evidenced by XRD analysis. The synthesized material showed complex mesoporous structures as indicated by the adsorption-desorption isotherms. XPS results revealed the existence of cerium and praseodymium in both +3 and +4 chemical valence states. Ceria-based materials represent an exciting class of catalysts for the combustion of soot. Catalytic evaluations showed that bare ceria-zirconia can also catalyze carbon combustion. Increasing the amount of cerium lowered the soot oxidation temperature. The catalyst containing 12 wt% praseodymium was capable of lowering the temperature of carbon oxidation from 634 to 434 °C. The high activity of soot oxidation could be due to the improved redox properties and the synergistic effects of praseodymium metal and the ceria-zirconia components as these catalysts showed higher activity compared to the unsupported forms. Further studies will be focused on the mechanism of soot oxidation with Pr-modified ceria-zirconia catalysts.

ACKNOWLEDGEMENTS

The authors thank Basic Scientific Research (UGC) for

the financial support.

REFERENCES

- Adams, K., Avataio, J., Sale, T., Rimkus, W., Hammerle, R. (1996) Laboratory screening of diesel oxidation catalyst and validation with vehicle testing: the importance of hydrocarbon storage. *SAE Transactions*, **105(4)**, 1978-1986.
- Prasad, R., Bella, V. R. (2011) Isothermal Kinetics of Catalyzed Air Oxidation of Diesel Soot. *Bulletin of Chemical Reaction Engineering & Catalysis*, **5(2)**, 95-101.
- Castoldi, L., Matarrese, R., Lietti, L., Forzatti, P. (2009) Intrinsic Reactivity of Alkaline and Alkaline-Earth Metal Oxide Catalysts for Oxidation of Soot. *Appl Catal B: Environ.*, **90(1-2)**, 278-285.
- Atribak, I., Bueno-Lopez, A., Garcia-Garcia, A. (2008) Thermally stable ceria-zirconia catalysts for soot oxidation by O₂. *Catalysis Communications*, **9(2)**, 250-255.
- Bueno-Lopez, A., Krishna, K., Makkee, M., Moulijn, A. J. (2005) Active oxygen from CeO₂ and its role in catalysed soot oxidation. *Catalysis Letters*, **99(3)**, 203-205.
- Reddy, B. M., Bharali, P., Thrimurthulu, G., Saikia, P., Katta, L., Park, S. E. (2008) Catalytic efficiency of ceria-zirconia and ceria-hafnia nanocomposite oxides for soot oxidation. *Catalysis Letters*, **123(3)**, 327-333.
- Neelapala, S. D., Dasari, H. (2018) Catalytic soot oxidation activity of Cr-doped ceria (Ce Cr O₂-δ)

- synthesized by sol-gel method with organic additives. *Materials Science for Energy Technologies*, **1(2)**, 155–159.
8. Eleonora Aneggi and Alessandro Trovarelli (2020) Potential of Ceria-Zirconia-Based Materials in Carbon Soot Oxidation for Gasoline Particulate Filters. *Catalysts*, **10(7)**, 768–781.
 9. Tahrizi Andana, Marco Piumetti, Samir Bensaid, Nunzio Russo, Debora Fino and Raffaele Pirone (2016) CO and Soot Oxidation over Ce-Zr-Pr Oxide Catalysts. *Nanoscale Research Letters*, **11**, 278–287.
 10. Jen, H. W., Graham, G. W., Chun, W., McCabe, R. W., Cuif, J. P., Deutsch, S. E., Touret, O. (1999) Characterization of model automotive exhaust catalysts. *Catalysis Today*, **50(2)**, 309–328.
 11. Sato, S., Koizumi, K., Nozaki, F. (1998) Ortho-selective methylation of phenol catalyzed by CeO₂-MgO prepared by citrate process. *Journal of catalysis*, **178(1)**, 264–274.
 12. Damyanova, S., Pawelec, B., Arishtirova, K., Huerta, M. V. M., Fierro, J. L. G. (2008) Study of the surface and redox properties of ceria-zirconia oxides. *Applied Catalysis A: General*, **337(1)**, 86–96.
 13. Yu, Q., Wu, X., Tang, C., Qi, L., Liu, B., Gao, F., Sun, K., Dong, L., Chen, Y. (2011) Textural, structural, and morphological characterizations and catalytic activity of nanosized CeO₂-MO_x (M = Mg²⁺, Al³⁺, Si⁴⁺) mixed oxides for CO oxidation. *Journal of Colloid and Interface Science*, **354(1)**, 341–352.
 14. Ramimoghadam, D., Hussein, M. Z., Taufiq-Yap, Y. H. (2012) The effect of sodium dodecyl sulfate (SDS) and cetyltrimethylammonium bromide (CTAB) on the properties of ZnO synthesized by hydrothermal method. *International journal of molecular sciences*, **13(10)**:13275–13293.
 15. Atribak, I., Bueno-López, A., García-García, A. (2009) Role of yttrium loading in the physico-chemical properties and sootcombustion activity of ceria and ceria/zirconia catalysts. *Journal of Molecular Catalysis A: Chemical*, **300(1-2)**, 103–110.
 16. Jian, L., Zhen, Z., Chunming, X., Aijun, D., Guiyuan, J. (2010) CeO₂-supported vanadium oxide catalysts for soot oxidation: the roles of molecular structure and nanometer effect. *Journal of rare earths*, **28(2)**, 198–204.
 17. Escribano, V. S., Lopez, E. F., Panizza, M., Resini, C., Amores, J. M. G., Busca, G. (2003) Characterization of cubic ceria-zirconia powders by X-ray diffraction and vibrational and electronic spectroscopy. *Solid State Sciences*, **5(10)**, 1369–1376.
 18. Cimi A. Daniel (2014) Ph. D thesis, Synthesis, characterization and catalytic activity of nanocrystalline ceria modified with zirconia. Cochin University of Science And Technology.
 19. Katta, L., Sudarsanam, P., Thrimurthulu, G., Reddy, M. B. (2010) Doped nanosized ceria solid solutions for low temperature soot oxidation: Zirconium versus lanthanum promoters. *Applied Catalysis B: Environmental*, **101(1-2)**, 101–108.
 20. Reddy, M. B., Reddy, K. G., Reddy, H. L., Ganesh, I. (2009) Synthesis of Nanosized Ceria-Zirconia Solid Solutions by a Rapid Microwave-Assisted Combustion Method. *The Open Physical Chemistry Journal*, **3**, 24–29.
 21. Cheng, D. G., Chong, M., Chen, F., Zhan, X. (2008) XPS characterization of CeO₂ catalyst for hydrogenation of benzoic acid to benzaldehyde. *Catalysis Letters*, **120**, 82–85.
 22. Wu, Q., Chen, J., Zhang, J. (2008) Effect of yttrium and praseodymium on properties of CeO₂-ZrO₂ solid solution for CH₄-CO₂ reforming. *Fuel Processing Technology*, **89(11)**, 993–999.
 23. Bharali (2009) Ph. D thesis, Design of novel nanosized ceria-based multicomponent composite oxides for catalytic applications. Osmania University.
 24. Reddy, B. M., Thrimurthulu, G., Katta, L., Yamada, Y., Park, S. E. (2009) Structural characteristics and catalytic activity of nanocrystalline ceria-praseodymia solid solutions. *The Journal of Physical Chemistry C*, **113(36)**, 15882–15890.
 25. Zhang, F., Chen, C. H., Hanson, J. C., Robinson, R. D., Herman, I. P., Chan, S. W. (2006) Phases in ceria-zirconia binary oxide (1-x) CeO₂-xZrO₂ nanoparticles: the effect of particle size. *Journal of the American Ceramic Society*, **89(3)**, 1028–1036.
 26. Aneggi, E., Leitenburg, C. D., Trovarelli, A. (2020) Influence of Nanoscale Surface Arrangements on the Oxygen Transfer Ability of Ceria-Zirconia Mixed Oxide. *Inorganics*, **8(34)**, 1–11.

27. Aneggi, E., de Leitenburg, C., Dolcetti, G., Trovarelli, A. (2006) Promotional effect of rare earths and transition metals in the combustion of diesel soot over CeO₂ and CeO₂-ZrO₂. *Catalysis Today*, **114**(1), 40–47.
28. Salem, I. A. (2000) Kinetics of the oxidative color removal and degradation of bromophenol blue with hydrogen peroxide catalyzed by copper (II)-supported alumina and zirconia. *Applied Catalysis B: Environmental*, **28**(3-4), 153–162.
29. Wu, X., Liu, D., Li, K., Li, J., Weng, D. (2007) Role of CeO₂-ZrO₂ in diesel soot oxidation and thermal stability of potassium catalyst. *Catalysis Communications*, **8**(8), 1274–1278.
30. P. Dulgheru J. A. Sullivan (2013) Rare Earth (La, Nd, Pr) Doped Ceria Zirconia Solid Solutions for Soot Combustion. *Top Catal.*, **56**, 504–510.
31. Atribak, I., López-Suárez, F. E., Bueno-López, A., García-García, A. (2011) New insights into the performance of ceria-zirconia mixed oxides as soot combustion catalysts. Identification of the role of “active oxygen” production. *Catalysis today*, **176**, 404-408.
32. Dhakad, M., Rayalu, S. S., Kumar, R., Doggali, P., Bakardjieva, S., Subrt, J., Mitsuhashi, T., Haneda, H., Labhsetwar, N. (2008) Low cost, ceria promoted perovskite type catalysts for diesel soot oxidation. *Catalysis Letters*, **121**, 137–143.
33. Weng, D., Li, J., Wu, X. D., Si, Z. (2011) Modification of CeO₂-ZrO₂ catalyst by potassium for NOx-assisted soot oxidation. *Journal of Environmental Sciences*, **23**, 145–150.